photonics

MDPI

Article

Raman Scattering Enhanced by Surface Plasmon Polaritons on Ag and Al Gratings

Ivan Z. Indutnyi, Viktor I. Mynko, Volodymyr M. Dzhagan, Andrii A. Korchovyi, Nazar V. Mazur *, Oleksandr M. Hreshchuk, Stanislav S. Serhiichuk, Volodymyr S. Yefanov and Volodymyr O. Yukhymchuk

V. Lashkaryov Institute of Semiconductor Physics, NAS of Ukraine, 41 Nauky Ave., 03028 Kyiv, Ukraine; mynkoviktor@gmail.com (V.I.M.); v.yukhymchuk@gmail.com (V.O.Y.)
* Correspondence: nazarmazur1994@gmail.com

Abstract

This paper describes the development and characterization of surface-enhanced Raman spectroscopy (SERS) substrates that employ the excitation of surface plasmon polaritons (SPPs) on periodic metal diffraction gratings to amplify the Raman signal of an analyte. The gratings were fabricated via interference photolithography on $As_{40}S_{40}Se_{20}$ thin films. The resulting surface relief was subsequently coated with either aluminium (Al gratings) or aluminium followed by silver (Ag gratings). The ratio of the relief depth to the grating period (*h*/*a*) was optimized to maximize SPP excitation efficiency. For both types of gratings, a strong angular dependence of the Raman scattering intensity of the analyte molecule (Rhodamine 6G) was observed, which anticorrelates with the angular dependence of the specularly reflected light intensity. The enhancement factor is 2×10^2 for the aluminium grating and 1×10^3 for the silver grating. This finding suggests that aluminium-based SERS substrates may serve as a cost-effective alternative to those coated with noble metals. Although the overall amplification is significantly lower than that achieved by SERS substrates based on localized surface plasmon (LSP) excitation, the grating-based SPP substrates offer a crucial advantage for quantitative measurements due to their uniform enhancement across the entire substrate area.

Keywords: SERS substrate; surface plasmon polaritons; silver (aluminium) diffraction gratings; interference photolithography; Raman scattering

1. Introduction

Surface-enhanced Raman spectroscopy (SERS) is an effective, non-destructive optical technique that provides detailed information about the vibrational structure of an analyte. This rapidly developing method is increasingly used for substance diagnostics across various fields, including chemistry, materials science, medicine, biology, pharmacology, and ecology [1–9].

SERS significantly enhances the Raman scattering signal—often by many orders of magnitude—when an analyte is deposited directly onto, or located in very close proximity (~1–2 nm) to metal nanostructures (NSs), typically silver (Ag) or gold (Au) [10]. This enhancement primarily stems from the excitation of surface plasmons in the metal NSs, in particular, localized surface plasmons (LSPs) in NSs and surface plasmon polaritons (SPPs) in flat metal films or nanogratings. A much less significant contribution comes from chemical enhancement [11,12], which occurs through the formation of chemical bonds between analyte molecules and the metal NSs, leading to the appearance of "shared

Check for updates

Received: 29 December 2025
Revised: 22 January 2026
Accepted: 27 January 2026
Published: 28 January 2026

Copyright: © 2026 by the authors. Licensee MDPI, Basel, Switzerland. This article is an open access article distributed under the terms and conditions of the Creative Commons Attribution (CC BY) license.

electrons" and new electronic states in the metal–analyte system. However, the electromagnetic mechanism (plasmon excitation) provides the dominant contribution to SERS signal enhancement [12].

The SERS substrate is the functional element that largely determines the method's sensitivity. Most common SERS substrates employ arrays of Au or Ag nanostructures of various sizes, shapes, and arrangements deposited on dielectric or semiconductor substrates. These structures rely on the excitation of LSPs by a specific laser wavelength, achieving record Raman signal enhancement [13], including single-molecule detection [14].

While Raman enhancement due to SPP excitation is generally lower than LSP-based enhancement, the advantage of the SPP approach is improved homogeneity of the signal across the substrate [15,16]. In LSP-based SERS, the major enhancement arises from a small number of "hot spots" randomly distributed across the substrate, resulting in highly nonuniform Raman amplification and, consequently, poor reproducibility that complicates quantitative analysis. In contrast, SPP-based SERS substrates provide nearly uniform Raman enhancement across their entire surface. This uniformity is achieved using thin, smooth metal layers deposited on flat or periodically profiled wafers, enabling efficient SPP excitation and greatly improving reproducibility. Given that reproducibility is often as important as high enhancement in many applications, SERS approaches based on SPP excitation have attracted considerable research interest in recent years [17–26].

Since SPPs cannot be excited under normal incidence, total internal reflection prisms in the Kretschmann or Otto configurations are traditionally used to excite SPPs on thin metal films. Consequently, much of the existing research on SPP-enhanced Raman scattering has focused on prism-based excitation schemes using flat substrates [18–23]. An alternative and particularly advantageous approach is the use of SERS substrates with a periodically profiled surface coated with a metal layer, such as diffraction gratings [24–28]. This method eliminates the need for a prism, simplifying the optical setup, as SPP excitation is achieved by direct illumination of the substrate. Matching of the wave vectors of the incident light and the SPPs is ensured by the contribution of the grating vector. Precise control over SPP excitation is achieved by varying the angle of incidence, the excitation wavelength, and the grating period. Theoretical and experimental studies [29–31] have shown that the efficiency of SPP excitation, and thus Raman enhancement, is primarily determined by the grating relief modulation depth, h/a, where h is the groove depth and a is the grating period.

In previous studies [24–28], gratings coated with noble metals were predominantly used for SPP excitation in SERS substrates. However, structures based on gold gratings are expensive, and silver gratings rapidly oxidize and degrade in air. At the same time, a number of studies have demonstrated that aluminium can serve as a promising plasmonic metal, potentially replacing gold, particularly in plasmon-polariton photodetectors [32,33]. Aluminum films oxidize rapidly in air at room temperature, forming a dense Al_2O_3 layer (3–4 nm thick), which protects the aluminum grating from further degradation. At the same time, the effect of such a thin Al_2O_3 layer on the SPP electromagnetic field strength at the analyte's location will be negligible.

Furthermore, although aluminum gratings exhibit lower initial enhancement than silver, they offer several advantages for SERS: plasmon resonance in the deep ultraviolet (DUV) range for biomolecule resonance enhancement, superior temporal stability due to a protective self-limiting Al_2O_3 layer, and broader plasmonic modes that ensure better spectral overlap with both excitation and Raman scattering.

Therefore, this work presents a comparative study of Raman enhancement efficiency for gratings with optimized modulation depth coated with either aluminium or silver. The aim of the study is to evaluate the feasibility of replacing silver gratings with aluminium ones as SERS substrates.

2. Materials and Methods

2.1. Substrate Fabrication

Holographic gratings for the SERS substrates were fabricated using interference photolithography. A 30-nm-thick chromium (Cr) adhesion layer and a 300-nm-thick $As_{40}S_{40}Se_{20}$ chalcogenide photoresist were sequentially deposited on polished glass wafers via thermal evaporation in a vacuum of 2×10^{-3} Pa. Film thicknesses were monitored in situ with a quartz thickness gauge and subsequently confirmed with a microinterferometer.

Periodic structures were recorded on the $As_{40}S_{40}Se_{20}$ film by projecting an interference pattern generated by a helium-cadmium laser (λ = 441.6 nm). Following exposure, selective wet etching of the photoresist layer formed a periodic relief of a controlled depth. Etching progress was monitored in situ by recording the diffraction of non-photoactive, long-wavelength radiation from the relief structure.

After rinsing and drying, the resulting gratings were coated with an 80-nm-thick Al layer via thermal vapour deposition. To create the silver grating samples, an additional 85-nm-thick Ag layer was applied to the Al-coated samples, also by thermal vapour deposition in a vacuum. As is known, silver, unlike aluminum, interacts with chalcogenide glasses, including $As_{40}S_{40}Se_{20}$, due to photo- and thermally stimulated diffusion. Therefore, in the Al-Ag bimetallic structure, aluminum plays the role of an insulating layer. Previous theoretical and experimental studies have shown that an Ag layer with a thickness of more than 80–90 nm is opaque in the visible region of the spectrum, while the field-enhancement factor for the electric field of SPP, as a function of silver film thickness, approaches saturation [34]. This determined the choice of metal layer thicknesses in the studied samples. The detailed fabrication method for such structures is described in our previous work [35].

AFM images of silver and aluminium gratings and their profiles are shown in Figure 1. They show that grains of different sizes form on the surface of aluminum and silver gratings. The RMS roughness measured from AFM is significantly smaller than the excitation wavelength and the grating periodicity. Therefore, although microroughness affects the absolute SERS intensity by slightly broadening the SPP resonance, its effect on the macroscopic signal uniformity remains negligible.

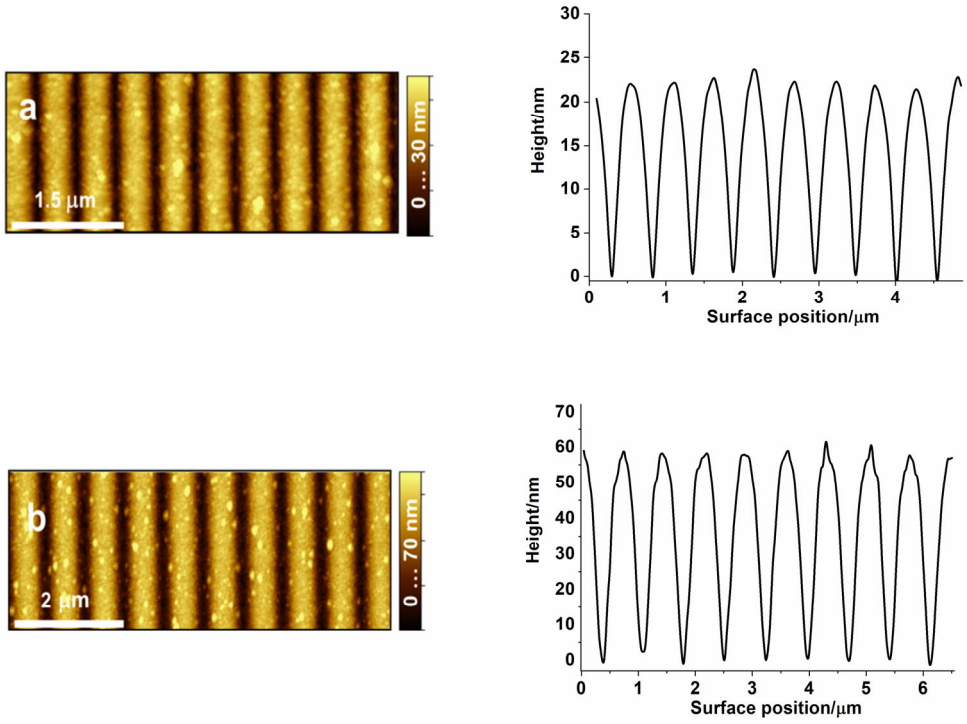


Figure 1. AFM images: silver grating and its profile (**a**); aluminium grating and its profile (**b**).

2.2. Characterization and Analyte Deposition

The profile shape and dimensions of the holographic gratings were determined using a NanoScope IIIa Dimension 3000 Scanning Atomic Force Microscope (Bruker Corp., Billerica, MA, USA). The spatial frequency of the gratings was measured with an accuracy of ±1 line/mm using an optical setup based on a G5M goniometer (LOMO, Saint Petersburg, Russia).

Rhodamine 6G (R6G), a standard analyte in SERS studies known for its strong resonant absorption in the 500–600 nm range, was used as the probe molecule. A thin layer of R6G was applied to the SERS substrates by wetting them in an aqueous solution of a specific concentration, 10^{-5} M, followed by drying.

2.3. Optical Measurements

To characterize the SPP resonance excitation efficiency both before and after analyte deposition, the specular reflectivity (*Rp*) of p-polarized He-Ne laser radiation (λ = 632.8 nm) was measured as a function of the incidence angle (θ). The angle θ is defined as the angle between the laser beam and the normal to the substrate plane. Measurements were performed on a setup incorporating a goniometer and a Fedorov stage (LOMO, Saint Petersburg, Russia). The sample was oriented such that the grating grooves were perpendicular to the plane of light incidence.

The effect of SPP excitation on the analyte's Raman spectra was investigated using the setup shown schematically in Figure 2. The setup comprised an MDR-23 monochromator equipped with a cooled iDus 401A CCD detector (Andor, UK), a CNI Model PSU-H-FDA solid-state laser, a collimator for collecting scattered Raman radiation, and a LaserCheck laser power meter. The spectra were excited using p-polarized laser radiation with a wavelength of 457 nm. The laser radiation was focused into a spot with a diameter of 25 μm. To prevent thermal or photo-induced sample modification, the radiation power density on the sample surface was kept below 10^3 W/cm^2. As our previous studies have shown, gratings based on $As_{40}S_{40}Se_{20}$, coated with an 80 nm thick aluminum layer, do not change their characteristics upon prolonged irradiation with a power of 5×10^3 W/cm^2 and also upon heating to 180 °C.

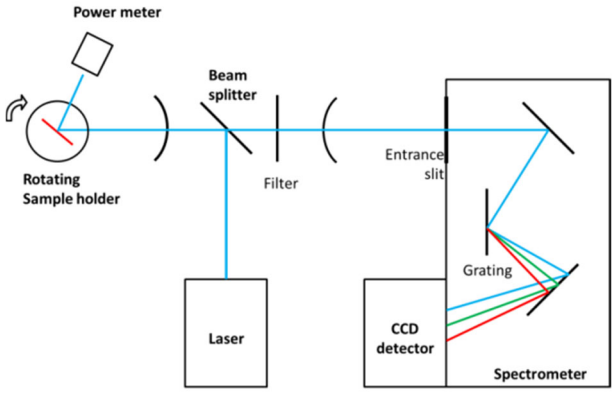


Figure 2. Schematic diagram of the setup for measuring SERS spectra and the intensity of specularly reflected excitation laser radiation at various angles of incidence on an analyte-coated grating. The grating is oriented such that the plane of incidence of the laser beam is perpendicular to its grooves.

The samples were mounted on a rotating platform, allowing for angle measurements with an accuracy of 0.1°. Light, scattered from the sample, was collected through an optical system (lenses, mirrors, and filters) and directed to the monochromator, where it was resolved into a spectrum by a diffraction grating and recorded by the CCD detector. With each sample rotation, the Raman spectrum and the power of the laser beam reflected from

the sample were recorded. The spectral resolution did not exceed 4 cm^{-1}. The phonon peak position of the silicon wafer (520.5 cm^{-1}) served as a reference for accurately determining the Raman peak positions.

3. Results and Discussion

3.1. Grating Parameters and SPP Resonance

As noted in the introduction, the efficiency of SPP excitation under resonant conditions on gratings is governed by the metal used for the plasmonic layer and the modulation depth (h/a). Previous work [36] established the maximum SPP excitation efficiency for silver-coated gratings (λ = 632.8 nm) at $h/a \approx 0.037$. For aluminium gratings, the optimal value is $h/a \approx 0.086$ [31].

In this study, we used a silver grating with a period of a = 519 nm and a relief depth of h = 21 nm, resulting in h/a = 0.04, which is close to the optimal value for silver (Figure 1a). The aluminium grating had a period of a = 694 nm and h/a = 0.083 (Figure 1b), also ensuring effective SPP excitation. Holographic gratings recorded on chalcogenide photoresist exhibit a profile shape that deviates slightly from a sinusoid, which, for shallow gratings like ours, can be accurately described by the sum of the first three harmonics of the Fourier expansion [37].

Figure 3 shows the angular dependence of the specular reflection coefficient (R_p) for p-polarized He-Ne laser radiation (λ = 632.8 nm) in air. Curves 1 and 2 correspond to the Al and Ag gratings, respectively. The figure clearly shows narrow minima in the reflection coefficient, which are characteristic of SPP excitation on the grating surfaces. The reflection coefficient dropping nearly to zero signifies the high efficiency of energy transfer from the incident light beam into the plasmon mode.

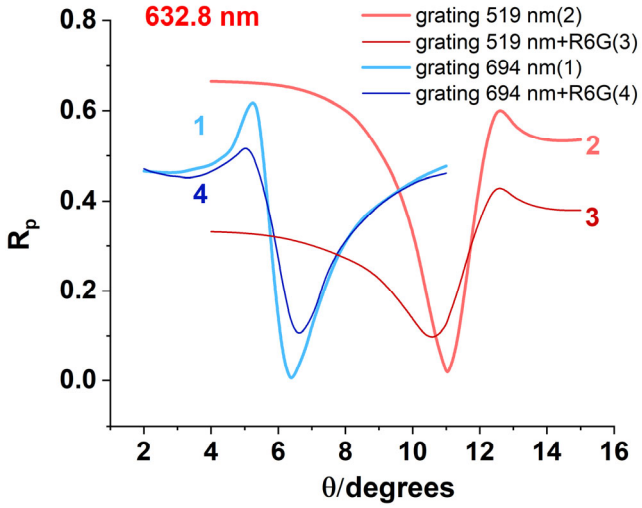


Figure 3. Dependence of the specular reflection coefficient R_p of p-polarized He-Ne laser radiation (λ = 632.8 nm) on the angle of incidence (θ) in the plasmon resonance region for an aluminium grating (a = 694 nm, curve 1) and a silver grating (a = 519 nm, curve 2). Curve 3 shows the angular dependence of R_p for the silver grating with a deposited layer of R6G, curve 4—the same for the aluminum grating.

Curve 3 in Figure 3 shows the angular dependence of R_p for the same silver grating (a = 519 nm) after depositing a thin layer of R6G. It is known that the deposition of a thin dielectric or semiconductor layer on a grating causes a shift in the SPP resonance [26]. For a grating with a period smaller than the probing wavelength (as in the case shown in Figure 3, curve 2), such a shift occurs in the direction of smaller angles (curve 3). For the case a > λ

(curve 1, aluminum grating), upon deposition of the R6G film, a shift in the R_p minimum in the opposite direction will be observed (curve 4).

3.2. Estimation of Film Thickness

The shift in the resonance angle is primarily determined by the optical density ($n_f \cdot d$) of the deposited dielectric film, where n_f is the film's refractive index and d is its thickness. The thickness d of the R6G film can be estimated by measuring the SPP resonance position before ($\theta_r{}^1$) and after ($\theta_r{}^2$) film deposition. We use the Homola formula [38], which relates the change in the effective refractive index of the SPPs (ΔN_{SPP}) to the film parameters, provided that the film thickness is much smaller than the plasmon field penetration depth ($d \ll l_d$):

$$\Delta N_{SPP} = \frac{2d}{l_d} \frac{N_{SPP}^3}{n^3} \Delta n \quad (1)$$

Here, $N_{SPP} = \mathrm{Re}\{k_{SPP}\}/k_0$ is the effective refractive index of the SPP; k_{SPP}—the wave vector of SPP; $k_0 = 2\pi/\lambda$ is the wave vector of the exciting radiation, n is the refractive index of the environment (air, $n = 1$), $\Delta n = n_f - n$. For a silver film in air at $\lambda = 632.8$ nm, the penetration depth $l_d \approx 419$ nm, confirming the applicability of Formula (1). ΔN_{SPP} is calculated using the scalar form of the quasi-momentum conservation condition [39]:

$$\mathrm{Re}(k_{SPP}) = nk_0 sin\theta \pm mG \quad (2)$$

where m (an integer $\neq 0$) is the diffraction order (here we will be limited to only the first diffraction order, m = 1) and $G = 2\pi/a$ is the grating vector. Using the literature value for the R6G refractive index $n_f = 1.92$ [40], and the experimentally measured resonance angles $\theta_r{}^1 = 11.1^\circ$ (curve 2) and $\theta_r{}^2 = 10.6^\circ$ (curve 3), we determine $\Delta N_{SPP} = \Delta \mathrm{Re}\{k_{SPP}\}/k_0$. Substituting this value into expression (1) yields a thickness of $d = 2 \pm 0.3$ nm for the R6G film. For the aluminum grating, using similar calculations, we obtained a very close thickness value for the R6G film: $d = 2.1 \pm 0.3$ nm. These samples were then used to study the effect of SPP excitation on the Raman signal enhancement.

3.3. Raman Enhancement via SPP Excitation

We first calculated the SPP excitation angles for the Ag and Al gratings using the $\lambda = 457$ nm laser radiation used for Raman excitation. Resonance occurs when the photon momentum and the surface plasmon momentum match, leading to strong light absorption and a minimum in the reflected beam intensity. The resonance angle is calculated using expression (2). Since gratings with a small modulation depth are investigated in this work, for an approximate estimate of the k_{SPP}, we used the expression obtained for the flat interface of semi-infinite media.

Using the dielectric constant for silver $\varepsilon_{Ag} = -7.5 + i \times 0.65$ at $\lambda = 457$ nm (from [41]), the theoretical angle for the silver grating ($a = 519$ nm) in air is $\theta \approx 11.1^\circ$. After depositing a rhodamine film with a thickness of $d = 2 \pm 0.3$ nm, the position of the plasmon resonance can be estimated using Formulas (1) and (2). The optical constants for the rhodamine fm (n = 1.27, absorption coefficient k = 0.19) for 457 nm are taken from [40]. We obtain the value $\theta = (11.56 \pm 0.8)^\circ$. For the aluminium grating (a = 694 nm), using $\varepsilon_{Al} = -3.7 + i \times 4.0$ at $\lambda = 457$ nm [41], the angle is calculated to be $\theta \approx 23.7^\circ$. With a 2 nm R6G layer, the similarly calculated value of the resonance angle for aluminum grating is $\theta = (24.7 \pm 0.9)^\circ$. The resonance angles increase slightly for both gratings, since when excited by radiation with $\lambda = 457$ nm, the relation $a > \lambda$ is satisfied in both cases.

Figure 4 shows the Raman spectra of R6G, measured in the 1400–1700 cm^{-1} spectral range, as a function of the incidence angle θ of the 457 nm laser radiation for the Ag and Al

gratings (Figures 4a and Figure 4b, respectively). The spectra clearly show seven bands, consistent with literature results [42–44].

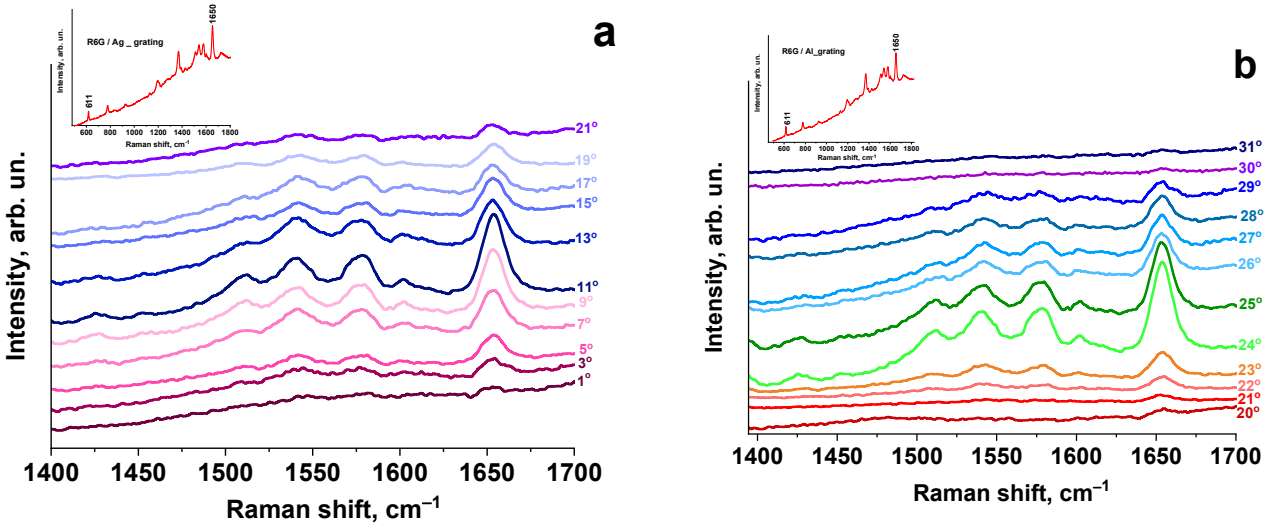


Figure 4. Raman spectra of the standard analyte R6G, deposited on SERS substrates representing diffraction gratings: (**a**) silver-coated (a = 519 nm) and (**b**) aluminium-coated (a = 694 nm). Spectra were excited by laser radiation with a wavelength of 457 nm. The angle of incidence of the exciting radiation varied from 1° to 31° with an accuracy of 0.1°. The insets to these figures show spectra in a wider spectral range.

The insets to these figures show spectra in a wider spectral range. Our experimental data shows that the ratio of the 1650 cm^{-1} band (aromatic C-C stretching) to the 611 cm^{-1} band (deformation in-plane) is approximately 3.75 for Ag grating and 3.0 for Al grating. According to SERS selection rules, this high I_{1650}/I_{611} ratio indicates a predominantly vertical or "edge" orientation of the R6G molecules on both Ag and Al gratings, although somewhat greater on silver. The latter is due to the formation of a thin layer of oxide on the aluminum grating. Importantly, this ratio remains constant within the measurement error regardless of the excitation angle, confirming that the observed differences in gain coefficients between silver and aluminum gratings reflect the intrinsic plasmonic efficiency of the metals.

The strong dependence of the Raman spectrum intensity on the incidence angle is clearly visible in Figure 4a.

This dependence is detailed in Figure 5a for the silver grating. Curve 1 (red colour) shows the angular dependence of the specularly reflected laser intensity, exhibiting a reflection minimum at $\theta \approx 11.5°$, which confirms the SPP excitation condition for the silver grating with the R6G layer at λ = 457 nm.

Curve 2 (black colour) shows the angular dependence of the intensity of the most prominent SERS band ($\nu \sim 1650$ cm^{-1}). A clearly pronounced maximum in the Raman scattering intensity is observed, and its angular position coincides precisely with the SPP resonance angle ($\theta \approx 11.5°$). Similar results for the aluminium grating (a = 694 nm) are shown in Figure 5b with the reflection minimum appearing at $\theta \approx 24.2°$ (Figure 5b, curve 1), which is in good agreement with the theoretical estimates given above. This position also coincides with the angular position of the maximum intensity of the SERS band ($\nu \sim 1650$ cm^{-1}) (curve 2). The intensity of the specularly reflected radiation at the minimum of the plasmon resonance for the silver grating is 2.8 mW, and for the aluminum grating is 3.2 mW. That is, the SPP excitation efficiencies for these gratings and at this wavelength are quite close in magnitude, but for the aluminum grating the efficiency is still somewhat lower.

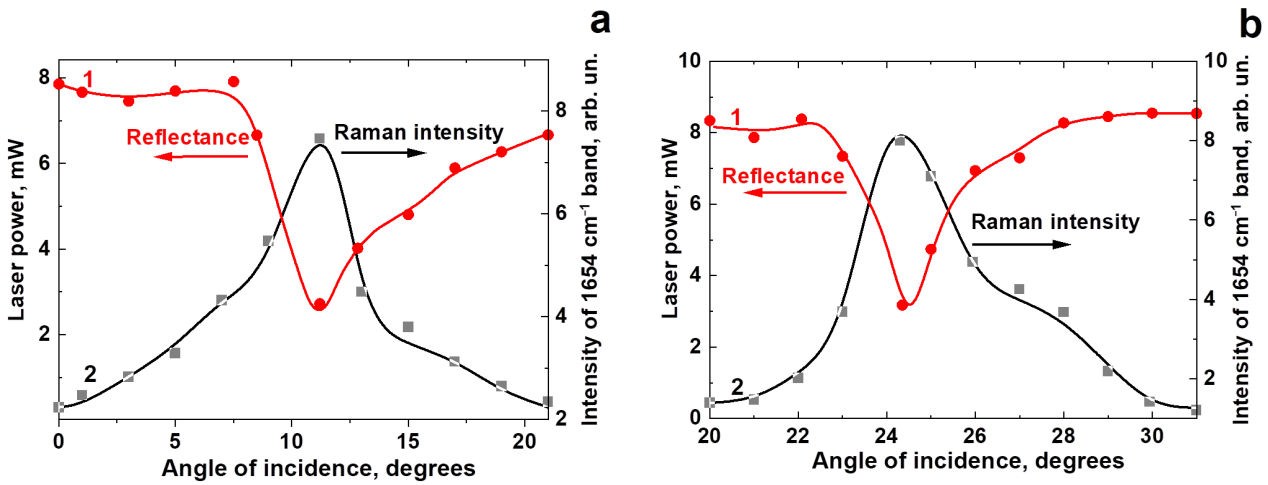


Figure 5. Angular dependences of the intensity of specularly reflected exciting radiation (curves 1) and the intensity of the SERS band (ν ~ 1650 cm^{-1}) of R6G molecules (curves 2) for excitation at λ = 457 nm: (**a**) silver grating (*a* = 519 nm); (**b**) aluminium grating (*a* = 694 nm). Dots and squares represent experimental values; solid lines represent their approximations.

3.4. Enhancement Factor Estimation

These results confirm that a significant enhancement of Raman scattering occurs on both silver and aluminium SERS substrates due to the excitation of SPPs on the grating surface. Importantly, the Raman signal was not recordable on similar flat-surface samples under identical R6G film application and measurement conditions. Furthermore, even on the studied grating samples, the Raman spectrum was not observed outside the SPP excitation angles.

To estimate the enhancement factor (k) of the Raman scattering signal for these laterally ordered Ag and Al gratings under SPP excitation, we compared the SERS signal to the normal Raman signal from R6G deposited on a silicon (Si) substrate. The comparison was conducted using the λ = 457 nm excitation in a back-scattering geometry, but with a significantly higher R6G concentration (~10^{-3} M) on the Si substrate to obtain a detectable signal.

Calculations show that to match the SERS intensity obtained from the silver and aluminium grating, the number of R6G molecules on the Si substrate would need to be 1×10^3 and 2×10^2 times greater, respectively. This yields enhancement factors of $k \approx 1 \times 10^3$ for the silver grating and $k \approx 2 \times 10^2$ for the aluminium grating. The enhancement factor is defined as [14]:

$$k = (I_{SERS}/N_{SERS})/(I_{Raman}/N_{Raman}), \quad (3)$$

where I and N are the measured intensity and the number of molecules, respectively. This definition accounts for the increase in the Raman signal per single molecule, as is standard for LSP-based SERS. (Note: SPP-amplified Raman signal is emitted directionally within a solid angle (the Kretschmann cone), which can lead to a significantly higher factor if calculated per unit spherical angle [25]). However, we adhere to the standard per-molecule definition.

The slightly higher enhancement factor for the silver grating can be partially attributed to the additional contribution from LSP resonance. The increase in surface area relative to a flat surface is nearly identical for both gratings and negligible. For the silver grating, the λ = 457 nm laser radiation excites LSP resonance because the maximum plasmon absorption for small Ag particles lies in the 380–450 nm range. In contrast, the plasmon absorption maximum for the aluminium grating is in the 150–200 nm range, so no additional amplification

from LSP resonance occurs under 457 nm excitation. At the same time, the character of the angular enhancement dependencies for both Ag and Al is remarkably similar (accounting for differences in permittivity). This similarity suggests that the fundamental physical nature of the enhancement in both cases is determined by the grating-driven excitation of SPPs. In our assessment, the LSP contribution in silver acts as an additional factor that explains its higher absolute efficiency compared to aluminum, but it does not alter the general physical framework of the comparison.

We also compared the obtained enhancement factors (EF) with the results published in the literature for similar periodic structures. For example, Kalachova et al. [24] reported EF values in the range of 10^2–1.6×10^4 for silver gratings optimized for visible light excitation, emphasizing the critical role of silver thickness and grating periodicity. In our work, the enhancement factor (EF) for the silver grating is 1×10^3, which is slightly less than the maximum value in [45], but we only varied the excitation angle of plasmon polaritons.

4. Conclusions

Diffraction gratings coated with silver (Ag) and aluminium (Al) layers were successfully fabricated using interference photolithography, demonstrating optimal modulation depths ($h/a \approx 0.04$ for Ag and $h/a \approx 0.083$ for Al) for effective surface plasmon polariton (SPP) excitation. Thin layers of the standard analyte, Rhodamine 6G (R6G), with a thickness of 2 ± 0.3 nm were deposited on these substrates.

Experimental results demonstrated that both grating types exhibit a strong angular dependence of the Raman scattering intensity that anticorrelates with the angular dependence of the intensity of specularly reflected exciting radiation. The experimentally determined angles for maximum Raman signal amplification agree with the SPP resonance angles.

The enhancement factor for the aluminium grating ($k \approx 2 \times 10^2$) is within the same order of magnitude as that for the silver grating ($k \approx 1 \times 10^3$). This suggests that aluminium SERS substrates offer a viable and cost-effective alternative to noble metal-coated gratings. An additional benefit of aluminium is its rapid oxidation in air, which forms a thin (3–4 nm), continuous layer of aluminium oxide. This oxide layer prevents further metal film degradation and provides the Al SERS substrate with sufficient wear resistance. While the enhancement factor is significantly lower than that achieved by localized plasmon (LSP) excitation, the primary advantage of these SPP-based gratings is the uniformity of the enhancement across the entire surface area. This characteristic makes them a highly valuable choice for quantitative SERS measurements, where reproducibility and spatial consistency are critical.

Author Contributions: Conceptualization, I.Z.I., V.I.M. and V.O.Y.; methodology, I.Z.I. and V.O.Y.; formal analysis, I.Z.I., V.M.D. and V.O.Y.; investigation, V.I.M., A.A.K., N.V.M., O.M.H. and S.S.S.; writing—original draft preparation, I.Z.I. and V.O.Y.; writing—review and editing, N.V.M. and V.S.Y.; supervision, I.Z.I., V.M.D. and V.O.Y.; funding acquisition, V.M.D. and V.O.Y. All authors have read and agreed to the published version of the manuscript.

Funding: V.M. Dzhagan and A.A. Korchovyi thanks for funding to the National Research foundation of Ukraine, grant # 2023.05/0022. All other authors were supported by the project #0125U000799 "New physical principles and technologies for the development of the element base of modern infrared photoelectronics" funded in the framework priority research programme of the NAS of Ukraine.

Data Availability Statement: All data supporting the findings of this study are included within the manuscript.

Conflicts of Interest: The authors declare no conflicts of interest.

References

1. Pilot, R.; Signorini, R.; Durante, C.; Orian, L.; Bhamidipati, M.; Fabris, L. A review on surface-enhanced raman scattering. *Biosensors* **2019**, *9*, 57. [CrossRef] [PubMed]
2. Lan, L.; Gao, Y.; Fan, X.; Li, M.; Hao, Q.; Qiu, T. The origin of ultrasensitive SERS sensing beyond plasmonics. *Front. Phys.* **2021**, *16*, 43300. [CrossRef]
3. Cupil-Garcia, V.; Strobbia, P.; Crawford, B.M.; Wang, H.-N.; Ngo, H.; Liu, Y.; Vo-Dinh, T. Plasmonic nanoplatforms: From surface-enhanced Raman scattering sensing to biomedical applications. *J. Raman Spectrosc.* **2020**, *52*, 541–553. [CrossRef]
4. Xie, W.; Schlucker, S. Medical applications of surface-enhanced Raman scattering. *Phys. Chem. Chem. Phys.* **2013**, *15*, 5329. [CrossRef]
5. Schlucker, S. Surface-enhanced Raman spectroscopy: Concepts and chemical applications. *Angew. Chem. Int. Ed.* **2014**, *53*, 4756. [CrossRef] [PubMed]
6. Aoki, P.H.B.; Furini, L.N.; Alessio, P.; Aliaga, A.E.; Constantino, C.J.L. Surface-enhanced Raman scattering (SERS) applied to cancer diagnosis and detection of pesticides, explosives, and drugs. *Rev. Anal. Chem.* **2013**, *32*, 55. [CrossRef]
7. Leona, M.; Stenger, J.; Ferloni, E. Application of surface-enhanced Raman scattering techniques to the ultrasensitive identification of natural dyes in works of art. *J. Raman Spectrosc.* **2006**, *37*, 981. [CrossRef]
8. Maleki, M.J.; Soroosh, M.; AL-Shammri, F.K.; Alkhayer, A.G.; Mondal, H. Design and Simulation of a Compact Subwavelength Graphene-Based Switch for Surface Plasmon Polariton Transmission in Integrated Optoelectronic Circuits. *Plasmonics* **2024**, *19*, 1701. [CrossRef]
9. Babicheva, V.E. Optical Processes behind Plasmonic Applications. *Nanomaterials* **2023**, *13*, 1270. [CrossRef]
10. Wang, H.-L.; You, E.-M.; Panneerselvam, R.; Ding, S.-Y.; Tian, Z.-Q. Advances of surface-enhanced Raman and IR spectroscopies: From nano/microstructures to macro-optical design. *Light. Sci. Appl.* **2021**, *10*, 161. [CrossRef] [PubMed]
11. Valley, N.; Greeneltch, N.; Van Duyne, R.P.; Schatz, G.C. A look at the origin and magnitude of the chemical contribution to the enhancement mechanism of surface-enhanced Raman spectroscopy (SERS): Theory and Experiment. *J. Phys. Chem. Lett.* **2013**, *4*, 2599. [CrossRef]
12. Tong, L.; Wei, H.; Zhang, S.; Xu, H. Recent Advances in Plasmonic Sensors. *Sensors* **2014**, *14*, 7959–7973. [CrossRef]
13. Pieczonka, N.P.W.; Aroca, R.F. Single molecule analysis by surfaced-enhanced Raman scattering. *Chem. Soc. Rev.* **2008**, *37*, 946. [CrossRef] [PubMed]
14. Nie, S.; Emory, S.R. Probing single molecules and single nanoparticles by surface-enhanced Raman scattering. *Science* **1997**, *275*, 1102–1106. [CrossRef]
15. Zalyubovskiy, S.J.; Bogdanova, M.; Deinega, A.; Lozovik, Y.; Pris, A.D.; An, K.H.; Hall, W.P.; Potyrailo, R.A. Theoretical limit of localized surface plasmon resonance sensitivity to local refractive index change and its comparison to conventional surface plasmon resonance sensor. *J. Opt. Soc. Am. A* **2012**, *29*, 994–1002. [CrossRef]
16. Mannelli, I.; Lecerf, L.; Guerrouache, M.; Goossens, M.; Millot, M.C.; Canva, M. DNA immobilisation procedures for surface plasmon resonance imaging (SPRI) based microarray systems. *Biosens. Bioelectron.* **2007**, *22*, 803–809. [CrossRef]
17. Meyer, S.A.; Auguie, B.; Le Ru, E.C.; Etchegoin, P.G. Combined SPR and SERS Microscopy in the Kretschmann Configuration. *J. Phys. Chem. A* **2012**, *116*, 1000–1007. [CrossRef]
18. Meyer, S.A.; Le Ru, E.C.; Etchegoin, P.G. Combining Surface Plasmon Resonance (SPR) Spectroscopy with Surface-Enhanced Raman Scattering (SERS). *Anal. Chem.* **2011**, *83*, 2337–2344. [CrossRef]
19. Ruiz-Sánchez, R.; Arencibia-Jorge, R.; Jiménez-Andrade, J.L.; Tagüeña, J.; Carrillo-Calvet, H.; Rubo, Y.G. Sixty Years of Research on Polaritons: A Scientometric Review. *Eng. Rep.* **2025**, *7*, e70045. [CrossRef]
20. Xu, S.; Liu, Y.; Li, H.; Xu, W. Surface-enhanced Raman scattering (SERS) based on surface plasmon resonance coupling techniques. *Front. Chem. China* **2011**, *6*, 341–354. [CrossRef]
21. Kim, J.-Y.; Zeng, Z.-C.; Xiao, L.; Schultz, Z.D. Elucidating Protein/Ligand Recognition with Combined Surface Plasmon Resonance and Surface Enhanced Raman Spectroscopy. *Anal. Chem.* **2017**, *89*, 13074–13081. [CrossRef] [PubMed]
22. Barchiesi, D.; Grosges, T.; Colas, F.; de la Chapelle, M.L. Combined SPR and SERS: Otto and Kretschmann configurations. *J. Opt.* **2015**, *17*, 114009. [CrossRef]
23. Beketov, G.V.; Shynkarenko, O.V.; Yukhymchuk, V.O. Optical arrangement for surface plasmon-assisted directional enhanced Raman scattering spectroscopy. *Spectrochim. Acta Part A* **2019**, *219*, 488–495. [CrossRef]
24. Kalachyova, Y.; Mares, D.; Lyutakov, O.; Kostejn, M.; Lapcak, L.; Švorčík, V. Surface Plasmon Polaritons on Silver Gratings for Optimal SERS Response. *J. Phys. Chem. C* **2015**, *119*, 9506–9512. [CrossRef]
25. Mathew, E.; Jenczyk, J.; Miłosz, Z.; Henzie, J.; Latsunskyi, I.; Florczak, P.; Andrzejewska, W.; Lewandowski, M.; Wiesner, M. Polarized-SERS of non-isotropic molecules on thermally-induced corrugated plasmonic surface supporting a NIR-SPP mode. *Appl. Surf. Sci.* **2024**, *659*, 159821. [CrossRef]

26. Deng, X.; Braun, G.B.; Liu, S.; Sciortino, P.F., Jr.; Koefer, B.; Tombler, T.; Moskovits, M. Single-Order, Subwavelength Resonant Nanograting as a Uniformly Hot Substrate for Surface-Enhanced Raman Spectroscopy. *Nano Lett.* **2010**, *10*, 1780–1786. [CrossRef] [PubMed]
27. Barelli, M.; Giordano, M.C.; Gucciardi, P.G.; de Mongeot, F.B. Self-Organized Nanogratings for Large-Area Surface Plasmon Polariton Excitation and Surface-Enhanced Raman Spectroscopy Sensing. *ACS Appl. Nano Mater.* **2020**, *3*, 8784−8793. [CrossRef]
28. Chen, Z.; Feng, K.; Chen, Z.; Shen, J.; Li, H. Surface-Enhanced Raman Scattering on Silver Sinusoidal Nanograting: Impact of Interactions of Grating-Coupled Surface Plasmon Polaritons. *Plasmonics* **2022**, *17*, 757–764. [CrossRef]
29. Maystre, D. Theory of Wood's Anomalies. In *Plasmonics*; Enoch, S., Bonod, N., Eds.; Springer Series in Optical Sciences 167; Springer-Verlag: Berlin/Heidelberg, Germany, 2012; Chapter 2.
30. Zaidi, S.H.; Yousaf, M.; Brueck, S.R.J. Grating coupling to surface plasma waves. First-order coupling. *J. Opt. Soc. Am. B* **1991**, *8*, 770–779. [CrossRef]
31. Indutnyi, I.Z.; Mynko, V.I.; Sopinskyy, M.V.; Dan'ko, V.A.; Lytvyn, P.M.; Korchovyi, A.A. Dependence of surface plasmon polyariton excitation efficiency on aluminum gratings relief depth. *Optoelectron. Semicond. Tech.* **2020**, *55*, 117–125. [CrossRef]
32. Lyaschuk, Y.; Indutnyi, I.; Myn'ko, V.; Romanyuk, V.; Mamontova, I.; Redko, R.; Dusheyko, M.; Savchuk, Y.; Tochkovyi, V.; Shtykalo, O.; et al. Aluminum-based plasmonic photodetector for sensing applications. *Appl. Sci.* **2024**, *14*, 4546. [CrossRef]
33. Mamykin, S.V.; Romanyuk, V.R.; Mynko, V.I.; Indutnyi, I.Z.; Redko, R.A.; Dusheyko, M.G.; Mamontova, I.B.; Lyaschuk, Y.M.; Savchuk, Y.M.; Shtykalo, O.V.; et al. Dust-insensitive smoke detector based on plasmon-polariton photodetector. *Semicond. Phys. Quantum Electron. Optoelectron.* **2024**, *27*, 466–471. [CrossRef]
34. Giannattasio, A.; Hooper, I.R.; Barnes, W.L. Transmission of light through thin silver films via surface plasmon-polaritons. *Opt. Express* **2004**, *12*, 5881. [CrossRef]
35. Dan'ko, V.; Indutnyi, I.; Min'ko, V.; Shepelyavyi, P. Interference photolithography with the use of resists on the basis of chalcogenide glassy semiconductors. *Optoelectron. Instrument. Proc.* **2010**, *46*, 483–490. [CrossRef]
36. Indutnyi, I.Z.; Mynko, V.I.; Sopinskyy, M.V.; Dan'ko, V.A.; Lytvyn, P.M. The effect of surface plasmon-polaritons on the photostimulated diffusion in light-sensitive Ag–As4Ge30S66 structures. *Semicond. Phys. Quantum Electron. Optoelectron.* **2021**, *24*, 436–443. [CrossRef]
37. Indutnyi, I.Z.; Mynko, V.I.; Sopinskyy, M.V.; Lytvyn, P.M.; Dan'ko, V.A. Excitation of Surface Plasmon Polaritons on Aluminum-Coated Diffraction Gratings Formed on an Inorganic Chalcogenide Photoresist: Influence of Profile Shape. *Plasmonics* **2022**, *17*, 2459–2466. [CrossRef]
38. Homola, J. Surface plamon resonance sensors for detection of chemical and biological species. *Chem. Rev.* **2008**, *108*, 462–493. [CrossRef] [PubMed]
39. Hibbins, A.P.; Sambles, J.R.; Lawrence, C.R. Azimuth-angle-dependent reflectivity data from metallic gratings. *J. Mod. Opt.* **1998**, *45*, 1019–1028. [CrossRef]
40. Seçkin, S.; Singh, P.; Jaiswal, A.; König, T.A.F. Super-Radiant SERS Enhancement by Plasmonic Particle Gratings. *ACS Appl. Mater. Interfaces* **2023**, *15*, 43124–43134. [CrossRef]
41. Palik, E.D. (Ed.) *Handbook of Optical Constants of Solids*; Academic Press: Cambridge, MA, USA, 1998; Volume III.
42. Hildebrandt, P.; Stockburger, M. Surface-enhanced resonance Raman spectroscopy of Rhodamine 6G adsorbed on colloidal silver. *J. Phys. Chem.* **1988**, *88*, 5935–5944. [CrossRef]
43. Weiss, A.; Haran, G. Time-dependent single-molecule Raman scattering as a probe of surface dynamics. *J. Phys. Chem. B* **2001**, *105*, 12348–12354. [CrossRef]
44. Watanabe, H.; Hayazawa, N.; Inouye, Y.; Kawata, S. DFT vibrational calculations of Rhodamine 6G adsorbed on silver: Analysis of tip-enhanced Raman spectroscopy. *J. Phys. Chem. B* **2005**, *109*, 5012–5020. [CrossRef] [PubMed]
45. Kahl, M.; Voges, E. Analysis of plasmon resonance and surface-enhanced Raman scattering on periodic silver structures. *Phys. Rev. B* **2000**, *61*, 14078. [CrossRef]

Disclaimer/Publisher's Note: The statements, opinions and data contained in all publications are solely those of the individual author(s) and contributor(s) and not of MDPI and/or the editor(s). MDPI and/or the editor(s) disclaim responsibility for any injury to people or property resulting from any ideas, methods, instructions or products referred to in the content.